metals

MDPI

Article

Structural and Corrosion Study of Uncoated and Zn-Cu Coated Magnesium-Based Alloy

Mehmet Yakup Hacıibrahimoğlu [1,*], Metin Bedir [2] and Abdulcabbar Yavuz [1]

[1] Metallurgical and Materials Science Engineering Department, Gaziantep University, Gaziantep 27310, Turkey; ayavuz@gantep.edu.tr

[2] Department of Engineering Physics, Gaziantep University, Gaziantep 27310, Turkey; bedir@gantep.edu.tr

* Correspondence: yakup@gantep.edu.tr; Tel.: +90-342-317-2240

Academic Editors: Adem Kurt, Necip Fazil Yilmaz and Halil Ibrahim Kurt

Received: 31 October 2016; Accepted: 14 December 2016; Published: 19 December 2016

Abstract: Zn-Cu alloy was deposited onto AZ63 substrate, and the corrosion behaviour of resulting modified electrodes was investigated in 3 wt % NaCl solution in comparison with uncoated AZ63. Electrochemical, structural, and morphological study of the coating is presented. SEM images reveal that the surface morphology of the films is uniformly small spherical grain distributions. The XRD patterns illustrate polycrystalline structure and the formation of peaks corresponding to hexagonal close-packed ε-phase of Zn-Cu with various crystallographic orientations. Cyclic voltammetry was used to determine the potential ranges where the various redox processes occur. Linear sweep voltammetry results illustrate that longer exposure of uncoated AZ63 in NaCl solution produces a greater corrosion potential shift because of the formation of an oxide layer that did not prevent the progression of corrosion attack. The corrosion resistivity of Zn-Cu coated AZ63 is approximately two orders of magnitude greater than that of uncoated AZ63.

Keywords: magnesium alloys; brass; electrodeposition; XRD; SEM; corrosion

1. Introduction

The consumption of magnesium as a non-ferrous alkaline earth metal has been used for transportation (aerospace, automobile), agriculture, chemical, construction, and energy industries, and even in medical applications thanks to its impressive properties, such as castability, weldability, good machinability, rigidity, toughness, and lightness [1]. In comparison with other materials used, the density of magnesium (1.74 g/cm^3) provides an advantage, as it is 35% lighter than aluminium and four times lighter than steel. Its low density means low inertia, which is also advantageous in rapidly moving components. Through alloying, the physical and chemical performance of pure Mg can be significantly increased [2]. However, Mg and Mg-based alloys suffer from a high corrosion rate (typically greater than 3 mm/year) [3].

As Mg-based alloys have wide range of probable applications, a good joining process of Mg and Mg-based alloys is required to combine dissimilar materials. The welding interface does not have different materials than the joining components [4]. Although mechanical and microstructural properties of the welding joints of Mg alloys have been widely studied [5], their corrosion problems have not been overcome. Corrosion phenomena of magnesium alloys is a serious limitation for their potential applications [6]. Specifically, the corrosion rate of magnesium-based alloys is low at atmospheric conditions [7]. Chloride-including media, however, cause a high corrosion rate of magnesium-based alloys [6,8]. Hence, the motivation of this paper is to deposit a well-known coating (brass) onto a Mg-based alloy, and to study its corrosion resistivity compared to a Mg-based alloy in NaCl solution. If the deposition process is successful and the corrosion resistivity of the film is higher than the Mg alloy, then a welding process applied to Mg-based alloys with similar or dissimilar joining

materials can be covered by a Zn-Cu modified electrode [9]. As the general corrosion behaviour of parent and welding nugget regions are the same, the coating of magnesium and welding of magnesium show the same trend [10,11].

The standard potential of Mg is more negative than any other engineering metal (including coatings) [12]. The corrosion potentials of Mg and its alloys are as negative as −2.4 V vs. normal hydrogen electrode and −1.7 V in aqueous solution due to $Mg(OH)_2$ formation [13]. The corrosion mechanism of Mg-based alloys in artificial seawater (3 wt % NaCl) as follows. The surface is covered by a partially protective film and then the corrosion of Mg (anodic reaction) [14] is formed at the breaks in the film as hydrogen liberation occurs with the cathodic reaction. The surface film formed on Mg-based alloys is not protective (not passivated), and the corrosion rate is more than 3 mm/year in a 3 wt % NaCl solution [3]. The type of magnesium corrosion is irregular localised corrosion [15], which spreads laterally across the surface of Mg-based alloys. As the cathodic reaction is hydrogen liberation, there is not much tendency for deep pitting [15]. The production of OH^- ions at the cathodic side of the reaction cause an increase in the value of pH and a decrease in corrosion tendency of Mg-based alloys, which is considered as a self-limiting reaction. The influence of pH and some ions (sulphates and chlorides) on the corrosion behaviour of pure magnesium was reported by Song et al. [16,17]. Corrosion studies have been conducted for Mg-based alloys by several research groups [18,19]. Among various surface treatments of magnesium alloys against corrosion, alloy coatings were extensively investigated [20]. Zinc-based coatings on Mg-based alloys can enhance corrosion resistivity, as zinc causes passivation [21,22].

Zn-Cu (brass) coatings are used for decorative purposes and to protect the substrates from aggressive media, including strong alkaline and acidic environments—environments which result in lifetime and performance reduction [23,24]. Cyanide-based solutions—which are not desirable due to environmental issues—were used as deposition electrolyte for Zn-Cu coatings in industry [25,26]. To solve these issues, environmentally-friendly and cyanide-free media including non-aqueous (ionic liquids [27] and deep eutectic solvents [28]) and aqueous media (gluconate [29], EDTA [30,31], mannitol [32], tartrate [33], ammonia [34], and pyrophosphate-based complex solutions [35,36]) have been used for Zn-Cu deposition. Specifically, pyrophosphate deposition bath is an environmentally friendly electrolyte [37], and metals/alloys obtained in this electrolyte do not produce their oxide/hydroxide forms [38–41]. As pyrophosphate bath is alkaline (pH > 9), and the corrosion resistivity of zinc coating deposited from alkaline electrolyte is increased, pyrophosphate bath was selected to coat the magnesium-based alloy in this study [42]. The aim of this study was to investigate the structural behaviour and corrosion resistivity of a magnesium-based alloy (AZ63) and Zn-Cu coated AZ63. As the Zn-Cu film was electrodeposited potentiostatically from pyrophosphate media, deposition and dissolution mechanisms of the film were also studied by means of cyclic voltammetry.

2. Experimental Section

The commercial composition of the AZ63 alloy was 90.8% Mg, 6.07% Al, 2.79% Zn, and 0.34% Mn. The disc-shaped Mg alloy working electrode substrates having an exposed area 1 cm in diameter was covered by a molded, compressed, and heated bakelite method. This is a conventional way to obtain the contact area and to isolate other sections of Mg alloy substrate from the electrolyte. The surface of the substrate was polished with a Struers-Laboforce-3 polishing set. Zn-Cu alloy was grown on the surface of the AZ63 substrates by using a traditional three electrode system. Pt flag and Ag/AgCl (saturated KCl) were used as working and reference electrodes, respectively. To grow the Zn-Cu alloys, the deposition baths were prepared from 0.90 M $K_4P_2O_7$ (Merck, Darmstadt, Germany), 0.15 M KH_2PO_4 (Sigma Aldrich, Steinheim, Germany), 0.20 M $ZnSO_4$ (Sigma Aldrich, Munich, Germany), and 0.02 M $CuSO_4$ (Sigma Aldrich, Munich, Germany) in double-distilled water (pH = 9.2). Films shown in this study were grown by applying −1.4 V for 300 s, and all experiments were conducted at room temperature.

The corrosion resistance measurements of Mg alloys before and after coating were performed in 3 wt % aqueous NaCl solution in the same Pyrex glass cell. In each measurement step, the specimens were ground mechanically with different high sensitive abrasive SiC papers (400, 800, 1200, 1500, 2000, and 3000) and cleaned in distilled water, then finally subjected to hot air drying process.

The quantitative composition analysis of the coatings was examined by a JEOL JSM 6390 LV scanning electron microscope (SEM, JEOL Ltd., Tokyo, Japan) with an energy dispersive spectrometer (EDX, JEOL Ltd., Tokyo, Japan) working at 15–30 kV. Preferential crystal orientations of the deposits on the AZ63 substrate were determined by X-ray diffraction (XRD) analysis, using a Philips PANalytical X'Pert Pro X-ray diffractometer (PANalytical, Almelo, The Netherlands) with Cu Kα radiation (1.5418 Å). The 2θ diffraction angle range of 30°–90° was recorded at a rate of 0.02° 2θ/0.5 s. The crystal phases were identified comparing the acquired 2θ values and their intensities. The potentiodynamic measurements for cyclic voltammetry and linear sweep voltammetry were examined to obtain the corrosion characteristics of coated and uncoated AZ63.

3. Results and Discussion

3.1. X-ray Diffraction Analysis

Figure 1 shows typical X-ray diffraction patterns of Zn-Cu deposition on AZ63 substrate obtained from a solution of copper and zinc salts in a potentiostatic process. The experimentally obtained crystal planes (hkl) were compared with the expected values for the phases described in JCPDS.

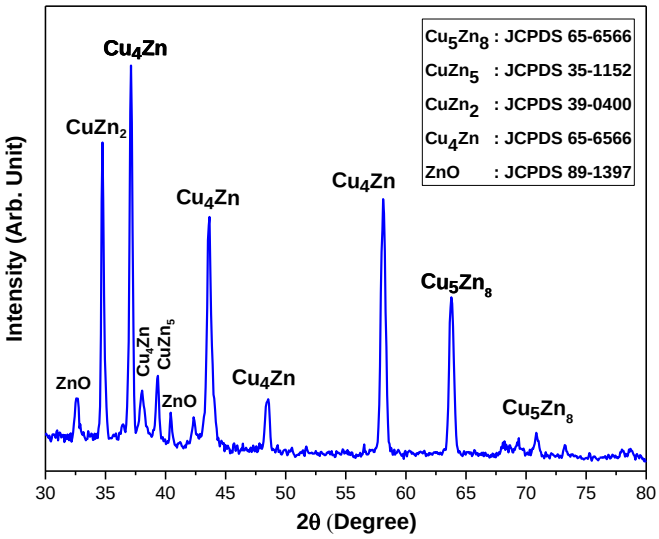

Figure 1. XRD pattern of Zn-Cu alloy growth on AZ63 substrate.

The dominant crystal orientation of the coating depends on the experimental conditions, such as pH, current density, and temperature. The XRD pattern shows the formation of lines corresponding to ZnO phase, hexagonal close packed ε-phase, and Zn-Cu phase, with different crystallographic orientations, and the film has polycrystalline structures. The highest intensity peaks were observed at 2θ values of 34.74°, 37.12°, 43.65°, 58.10°, and 63.78°. These were well indexed to the planes of $CuZn_2$, $Cu_{0.8}Zn_{0.2}$, $Cu_{0.8}Zn_{0.2}$, $Cu_{0.8}Zn_{0.2}$, and Cu_5Zn_8, respectively. There were also lower intensity peaks observed at the angles (2θ) of 32.56°, 37.7°, 38.9°, 41.4°, 48.53°, and 72.03°. These were indexed to the planes of ZnO, $Cu_{0.8}Zn_{0.2}$, $CuZn_5$, ZnO, $Cu_{0.8}Zn_{0.2}$, and Cu_5Zn_8, respectively. The observed phase as expected is based on the binary equilibrium diagram of the Zn-Cu system. Figure 1 shows that peaks are generally indexed to the diffractions of intermetallic ε phase of Zn-Cu, which is known to have the composition of $Cu_{0.8}Zn_{0.2}$. The peak intensity is in planes of hexagonal phase and was observed to be high for Zn-Cu, which indicates the crystallinity of a Zn-Cu alloy.

3.2. Scanning Electron Microscope Analysis

Figure 2 shows the results of the Zn-Cu coated AZ63 surface morphology and elemental analysis by means of SEM and EDX. The Zn-Cu film—grown from the concentration of $ZnSO_4$ (0.1 M) and that of $CuSO_4$ (0.01 M) in pyrophosphate deposition bath—had 82.9 wt % Zn and 17.1 wt % Cu.

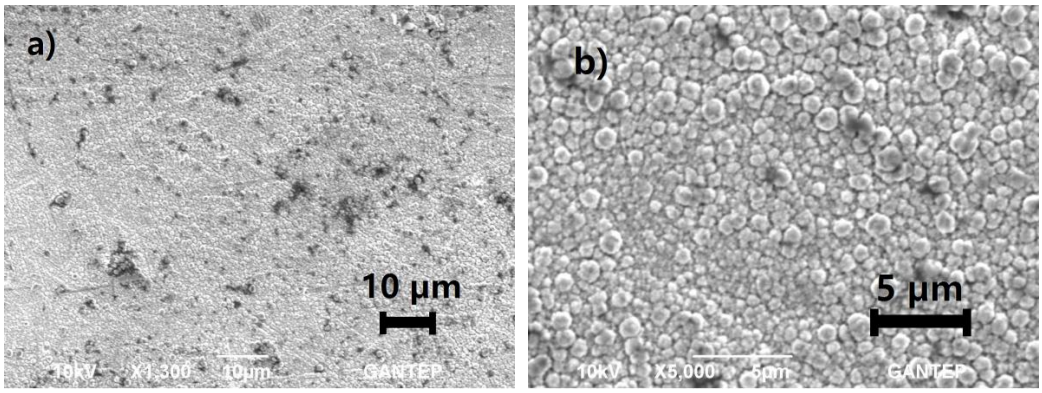

Figure 2. Different magnified SEM images of Zn-Cu coated AZ63 alloy (**a**) 1300× and (**b**) 5000×.

Figure 2a,b shows the different magnified images of Zn-Cu coated AZ63. The microstructure of the films consists of different spherical grains distributed uniformly throughout the surface. The intermetallic precipitates have an average diameter between 0.5 µm and 2 µm. As the coating of the precipitate appears compact and uniform, the coating on the matrix appeared uncracked and regular. This is the typical characteristic of a Zn-Cu alloy coated surface [43,44].

3.3. Cyclic Voltammetry Analysis

The cyclic voltammogram shown in Figure 3 was obtained for AZ63 working electrode in the solution mentioned in the experimental section. The first cathodic peak seen at around −0.4 V is attributed to the reduction of Cu^{2+} to Cu^{+}. Further reduction continuing rapidly at around −1.3 V is due to the reduction of Cu^{+} to solid Cu, associated with the reduction of solid Zn from Zn^{2+} [45]. The same cyclic voltammograms were obtained from the solution containing zinc and copper electrolyte having a ligand [46]. Indeed, hydrogen evolution also occurs with co-deposition of the Zn-Cu alloy [43]. The hydrogen revealed during co-deposition of Zn-Cu alloy, however, does not affect Zn-Cu composition, as shown in the XRD results.

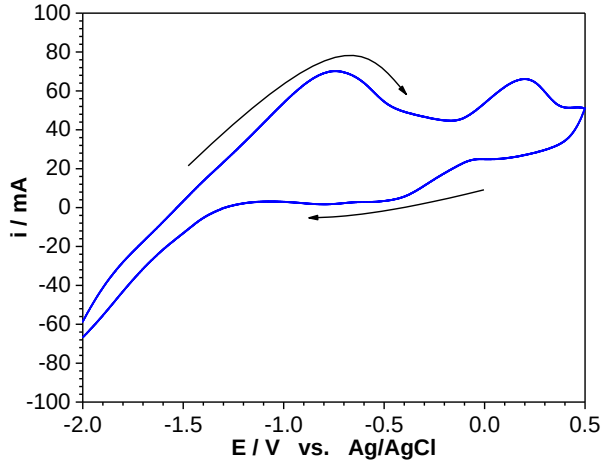

Figure 3. Cyclic voltammogram of AZ63 obtained from electrolytic solution between −2.0 V and +0.5 V at the scan rate of 100 $mV \cdot s^{-1}$.

The film includes various oriented crystals consisting of only Zn-Cu alloy (see XRD section). On the reverse direction, the Zn-Cu alloy coating is stripped. The peak at around −0.8 V is associated to the oxidation of solid Zn (Zn^0) to Zn^{2+} and Cu^0 to Cu^+. The other oxidation peak at around 0.2 V appears due to the oxidation of Cu^+ to Cu^{2+} [45]. After that potential, the entire Zn-Cu alloy is dissolved. Although electrochemically obtained Zn-Cu alloy deposition has already been studied [47,48], the work presented here focuses on the corrosion resistivity of the Zn-Cu film.

3.4. Linear Sweep Voltammetry Analyses of Uncoated and Zn-Cu Coated AZ63

To investigate the corrosion resistivity effect of the coating on AZ63, potentiodynamic anodic and cathodic polarization curves for Zn-Cu coated and uncoated AZ63 alloys immersed in a 3 wt % NaCl solution for different times are shown in Figure 4.

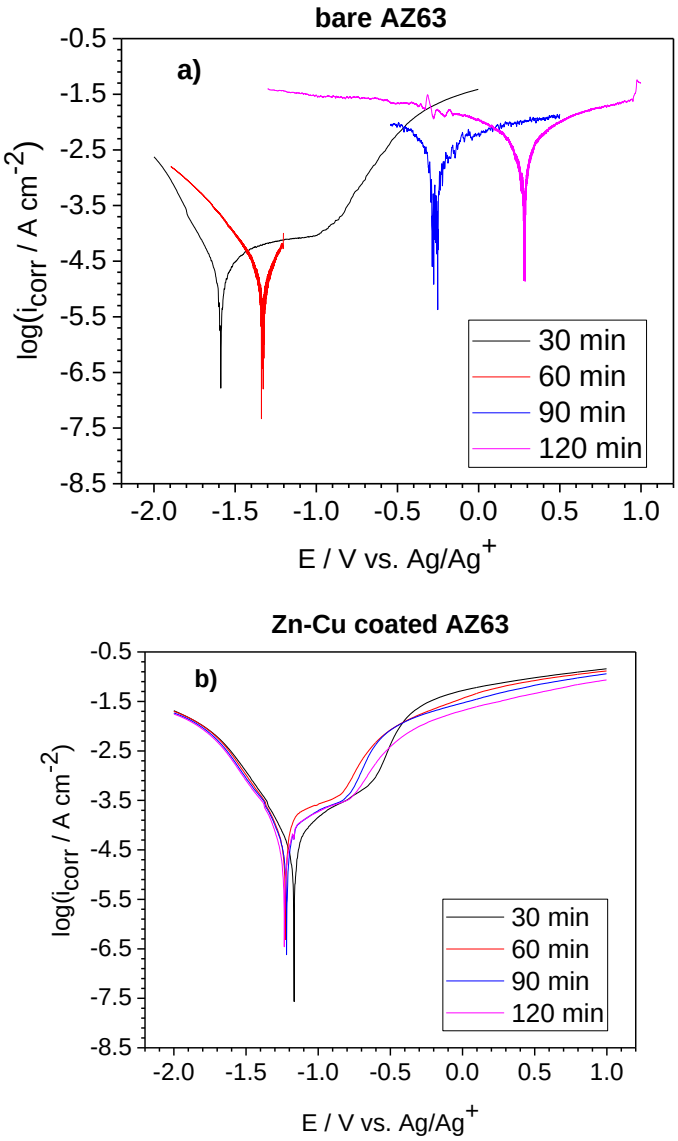

Figure 4. Potentiodynamic polarization curves for (**a**) uncoated AZ63 alloy and (**b**) Zn-Cu coated AZ63 in 3 wt % NaCl solution for 30, 60, 90, and 120 min.

Figure 4a shows that the anodic and cathodic polarisations in the NaCl solution are affected by the immersion time. Polarization curve of bare AZ63 immersed in NaCl solution for 30 min can be separated into three distinct regions. The first region is the cathodic polarization commencing

from −2.0 V, mainly due to hydrogen evolution. The second region is between E_{corr} (−1.6 V) and −0.9 V, in which there is no significant oxidation of the Mg-based alloy in the corrosive NaCl medium. However, it is obvious that the bare AZ63 had an oxidised reaction (as expected) in the NaCl solution after −0.9 V in the anodic direction, as the current increases dramatically at this region, corresponding to the third region. The corrosion potential (E_{corr}) and the corrosion current density (i_{corr}) for all data shown in Figure 4 are given in Table 1. The Tafel plot for the bare AZ63 film immersed in NaCl solution for 60 min is similar to that for 30 min. However, E_{corr} and i_{corr} values for the bare film immersed in NaCl solution for 90 and 120 min are significantly changed (see Table 1). The values of polarization resistance (R_p) given in Table 1 are inversely related to i_{corr} formulated by the Sterm-Geary equation in terms of the values of anodic (β_a) and cathodic (β_c) Tafel constants [49] (given in Equation (1)).

$$R_p = \frac{\beta_c \beta_a}{2.3 i_{corr}(\beta_c + \beta_a)} \quad (1)$$

E_{corr} of the film increases with exposure time due to the formation of a magnesium oxide layer [50]. Additionally, current density increases with exposure time in NaCl. While i_{corr} of the AZ63 immersed in NaCl solution for 30 min is 4.72 A·cm^{-2}, i_{corr} of that for 120 min is 2.33 A·cm^{-2} (from logarithmic calculation, it is 245 times more readily corroded, as 4677/19.1 = 245, given in Table 1). Increasing in current density with immersion time indicates that the AZ63 film has a pitting corrosion reaction in the NaCl media.

Table 1. E_{corr} and i_{corr} parameters extracted from Tafel plot of Figure 4 in artificial seawater. R_p is calculated from the Sterm-Geary equation.

Duration in 3 wt % NaCl	Uncoated AZ63 Alloy			Zn-Cu Coated AZ63 Alloy		
	E_{corr} (V)	i_{corr} (μA·cm^{-2})	R_p (Ω·cm^{-2})	E_{corr} (V)	i_{corr} (μA·cm^{-2})	R_p (Ω·cm^{-2})
30 min	−1.61	19.1	4336	−1.17	26.3	1791
60 min	−1.31	26.9	1957	−1.23	70.8	1082
90 min	−0.23	2754	17.8	−1.22	46.8	1664
120 min	+0.29	4677	18.5	−1.23	49.0	1663

Figure 4b presents the polarisation curves of Zn-Cu coated Mg-based alloy at different exposure times in the same corrosive electrolyte (3 wt % aqueous NaCl solution) used for uncoated AZ63. The values of corrosion potential and corrosion current density for Zn-Cu coated AZ63 are nearly unchanged with different duration. There is a significant shift towards positive potential values from −1.61 V to +0.29 V (voltage difference is 1.90 V) for uncoated AZ63 in NaCl solution. However, the voltage difference of Zn-Cu coated AZ63 between 30 min and 120 min is only 0.06 V, meaning that Zn-Cu coated AZ63 shows higher resistance than uncoated AZ63 against corrosion. Each polarisation curve of coated AZ63 in NaCl bath for varied immersion times given in Figure 4b has identical oxidation behaviour that is similar to that of uncoated AZ63 in NaCl for 30 min (black line of Figure 4b). The similarity between Zn-Cu coated AZ63 curves given Figure 4b indicates that Zn-Cu coating prevents the pitting corrosion of AZ63.

i_{corr} for uncoated AZ63 and Zn-Cu coated AZ63 are 4677 μA·cm^{-2} and 49 μA·cm^{-2}, respectively. Therefore, the corrosion rate of Zn-Cu coating is 96 times less than that of the bare alloy. This difference is due to the passivation and pitting behaviour of the surfaces. Uncoated AZ63 has pitting corrosion. The results of corrosion resistivity calculated from corrosion rate have the opposite trends with polarisation resistance, as expected (see Table 1). When AZ63 is coated with Zn-Cu, its surface is protected against corrosion, because this protective film creates a barrier between the Mg-based alloy and the corrosive medium during the electrochemical process. The Zn-Cu alloy can be simply deposited onto different metals/alloys, including steel [43,45], nickel [51], and copper [52] based materials. If Mg-based alloys are welded (by friction stir welding) to other materials, Zn-Cu alloy coating can be deposited onto both dissimilar components and joint to protect them from corrosion.

The corrosion behaviour of magnesium-based alloys (AZ31 and AZ61) deduced from hydrogen evolution in 0.6 M NaCl has similar trends as obtained from the electrochemical polarisation data [53].

4. Conclusions

In this study, the structural, morphological, and corrosion behaviour of uncoated and Zn-Cu alloy-coated AZ63 substrate were investigated. The formation of peaks corresponding to hexagonal close-packed ε-phase of Zn-Cu with different crystallographic orientations were observed, indicating that the film is in a polycrystalline structure. According to microstructural analysis of the films, the surface of coated AZ63 alloy consists of uniformly distributed spherical grains between 0.5 μm and 2 μm in diameter.

The electroplating behaviour and corrosion characteristics were examined using cyclic and linear sweep voltammetric measurements. There is a significant change in the values of corrosion potential and corrosion current density for uncoated AZ63 in the NaCl solution. However, the values of E_{corr} and i_{corr} for Zn-Cu coated AZ63 remain unchanged with different immersion time in NaCl bath. AZ63 has pitting corrosion reaction in the NaCl media, and the corrosion is accelerated with immersion time of AZ63 in the chloride-based medium. Zn-Cu coating creates a barrier between Mg-based alloy and electrolyte and hence protects AZ63 against corrosion in the corrosive chloride environment. This study suggests that welded Mg-based alloys with similar/dissimilar materials can be protected against corrosion by a Zn-Cu coating.

Acknowledgments: This study is supported by University of Gaziantep, Scientific Research Projects Unit (BAPYB) by a research project number of MF.YLT.1608. The Authors would like to thank to Food Products R&D Centre, Gaziantep University.

Author Contributions: M.Y.H. and M.B. conceived and designed the experiments; M.Y.H. performed the experiments; M.Y.H., M.B. and A.Y. analysed the data; M.Y.H. and A.Y. wrote the paper.

Conflicts of Interest: The authors declare no conflict of interest.

References

1. Gupta, M.; Sharon, N.M.L. *Magnesium, Magnesium Alloys, and Magnesium Composites*; John Wiley & Sons: Somerset, NJ, USA, 2011; pp. 1–11.
2. Forsmark, J.H.; Dowling, Z.; Gibson, K.; Mueller, C.; Godlewski, L.; Zindel, J.; Boileau, J. An investigation of the effects of cast skin on the mechanical properties of an AM60 die-cast magnesium alloy. *SAE Int. J. Mater. Manuf.* **2015**, *8*, 714–721. [CrossRef]
3. Candan, S.; Unal, M.; Turkmen, M.; Koc, E.; Turen, Y.; Candan, E. Improvement of mechanical and corrosion properties of magnesium alloy by lead addition. *Mater. Sci. Eng. A* **2009**, *501*, 115–118. [CrossRef]
4. Fu, B.; Qin, G.; Li, F.; Meng, X.; Zhang, J.; Wu, C. Friction stir welding process of dissimilar metals of 6061-T6 aluminum alloy to AZ31B magnesium alloy. *J. Mater. Process.Technol.* **2015**, *218*, 38–47. [CrossRef]
5. Mishra, R.S.; Ma, Z. Friction stir welding and processing. *Mater. Sci. Eng. R Rep.* **2005**, *50*, 1–78. [CrossRef]
6. Song, G.; Atrens, A.; Stjohn, D.; Nairn, J.; Li, Y. The electrochemical corrosion of pure magnesium in 1 N NaCl. *Corros. Sci.* **1997**, *39*, 855–875. [CrossRef]
7. Song, G.L.; Atrens, A. Corrosion mechanisms of magnesium alloys. *Adv. Eng. Mater.* **1999**, *1*, 11–33. [CrossRef]
8. Inoue, H.; Sugahara, K.; Yamamoto, A.; Tsubakino, H. Corrosion rate of magnesium and its alloys in buffered chloride solutions. *Corros. Sci.* **2002**, *44*, 603–610. [CrossRef]
9. Liu, L.; Ren, D.; Liu, F. A review of dissimilar welding techniques for magnesium alloys to aluminum alloys. *Materials* **2014**, *7*, 3735–3757. [CrossRef]
10. Commin, L.; Dumont, M.; Masse, J.E.; Barrallier, L. Friction stir welding of AZ31 magnesium alloy rolled sheets: Influence of processing parameters. *Acta Mater.* **2009**, *57*, 326–334. [CrossRef]
11. Laser, T.; Nürnberg, M.R.; Janz, A.; Hartig, C.; Letzig, D.; Schmid-Fetzer, R.; Bormann, R. The influence of manganese on the microstructure and mechanical properties of AZ31 gravity die cast alloys. *Acta Mater.* **2006**, *54*, 3033–3041. [CrossRef]

12. Song, G.; Atrens, A. Understanding magnesium corrosion—A framework for improved alloy performance. *Adv. Eng. Mater.* **2003**, *5*, 837–858. [CrossRef]
13. Ambat, R.; Aung, N.N.; Zhou, W. Evaluation of microstructural effects on corrosion behaviour of AZ91D magnesium alloy. *Corros. Sci.* **2000**, *42*, 1433–1455. [CrossRef]
14. Thomas, S.; Medhekar, N.; Frankel, G.; Birbilis, N. Corrosion mechanism and hydrogen evolution on Mg. *Curr. Opin. Solid State Mater. Sci.* **2015**, *19*, 85–94. [CrossRef]
15. Ročňáková, I.; Montufar, E.B.; Horynová, M.; Zikmund, T.; Novotný, K.; Klakurková, L.; Čelko, L.; Song, G.-L.; Kaiser, J. Assessment of localized corrosion under simulated physiological conditions of magnesium samples with heterogeneous microstructure: Value of X-ray computed micro-tomography platform. *Corros. Sci.* **2016**, *104*, 187–196. [CrossRef]
16. Song, G.; Atrens, A.; St. John, D.; Wu, X.; Nairn, J. The anodic dissolution of magnesium in chloride and sulphate solutions. *Corros. Sci.* **1997**, *39*, 1981–2004. [CrossRef]
17. Song, G.; Atrens, A.; Wu, X.; Zhang, B. Corrosion behaviour of AZ21, AZ501 and AZ91 in sodium chloride. *Corros. Sci.* **1998**, *40*, 1769–1791. [CrossRef]
18. Ambat, R.; Aung, N.N.; Zhou, W. Studies on the influence of chloride ion and pH on the corrosion and electrochemical behaviour of AZ91D magnesium alloy. *J. Appl. Electrochem.* **2000**, *30*, 865–874. [CrossRef]
19. Altun, H.; Sen, S. Studies on the influence of chloride ion concentration and pH on the corrosion and electrochemical behaviour of AZ63 magnesium alloy. *Mater. Des.* **2004**, *25*, 637–643. [CrossRef]
20. Gray, J.; Luan, B. Protective coatings on magnesium and its alloys—A critical review. *J. Alloy. Compd.* **2002**, *336*, 88–113. [CrossRef]
21. Song, G.; Johannesson, B.; Hapugoda, S.; StJohn, D. Galvanic corrosion of magnesium alloy AZ91D in contact with an aluminium alloy, steel and zinc. *Corros. Sci.* **2004**, *46*, 955–977. [CrossRef]
22. Lian, J.S.; Li, G.Y.; Niu, L.Y.; Gu, C.D.; Jiang, Z.H.; Jiang, Q. Electroless Ni–P deposition plus zinc phosphate coating on AZ91D magnesium alloy. *Surf. Coat. Technol.* **2006**, *200*, 5956–5962. [CrossRef]
23. Ebrahimzadeh, M.; Gholami, M.; Momeni, M.; Kosari, A.; Moayed, M.; Davoodi, A. Theoretical and experimental investigations on corrosion control of 65Cu–35Zn brass in nitric acid by two thiophenol derivatives. *Appl. Surf. Sci.* **2015**, *332*, 384–392. [CrossRef]
24. Jie, H.; Xu, Q.; Wei, L.; Min, Y. Etching and heating treatment combined approach for superhydrophobic surface on brass substrates and the consequent corrosion resistance. *Corros. Sci.* **2016**, *102*, 251–258. [CrossRef]
25. Banerjee, T.; Allmand, A. Experiments on the electrodeposition of brass from cyanide solutions. *Trans. Faraday Soc.* **1948**, *44*, 819–833. [CrossRef]
26. Vagramyan, T.; Leach, J.; Moon, J. On the problems of electrodepositing brass from non-cyanide electrolytes. *Electrochim. Acta* **1979**, *24*, 231–236. [CrossRef]
27. Schütte, K.; Meyer, H.; Gemel, C.; Barthel, J.; Fischer, R.A.; Janiak, C. Synthesis of Cu, Zn and Cu/Zn brass alloy nanoparticles from metal amidinate precursors in ionic liquids or propylene carbonate with relevance to methanol synthesis. *Nanoscale* **2014**, *6*, 3116–3126. [CrossRef] [PubMed]
28. De Vreese, P.; Skoczylas, A.; Matthijs, E.; Fransaer, J.; Binnemans, K. Electrodeposition of copper–zinc alloys from an ionic liquid-like choline acetate electrolyte. *Electrochim. Acta* **2013**, *108*, 788–794. [CrossRef]
29. Survila, A.; Mockus, Z.; Kanapeckaitė, S.; Stalnionis, G.; Juškėnas, R.; Jasulaitienė, V. Codeposition of zinc and copper in gluconate-sulfate solutions. *J. Electrochem. Soc.* **2013**, *160*, D428–D433. [CrossRef]
30. De Almeida, M.R.H.; Barbano, E.P.; Zacarin, M.G.; de Brito, M.M.; Tulio, P.C.; Carlos, I.A. Electrodeposition of cuzn films from free-of-cyanide alkaline baths containing edta as complexing agent. *Surf. Coat. Technol.* **2016**, *287*, 103–112. [CrossRef]
31. De Almeida, M.; Barbano, E.; de Carvalho, M.; Carlos, I.; Siqueira, J.; Barbosa, L. Electrodeposition of copper–zinc from an alkaline bath based on edta. *Surf. Coat. Technol.* **2011**, *206*, 95–102. [CrossRef]
32. Juškėnas, R.; Karpavičienė, V.; Pakštas, V.; Selskis, A.; Kapočius, V. Electrochemical and xrd studies of Cu–Zn coatings electrodeposited in solution with d-mannitol. *J. Electroanal. Chem.* **2007**, *602*, 237–244. [CrossRef]
33. Domínguez-Ríos, C.; Moreno, M.; Torres-Sánchez, R.; Antúnez, W.; Aguilar-Elguézabal, A.; González-Hernández, J. Effect of tartrate salt concentration on the morphological characteristics and composition of Cu-Zn electroless plating on zamak 5 zinc alloy. *Surf. Coat. Technol.* **2008**, *202*, 4848–4854. [CrossRef]

34. Ibrahim, M.A.; Bakdash, R.S. New cyanide-free ammonia bath for brass alloy coatings on steel substrate by electrodeposition. *Int. J. Electrochem. Sci.* **2015**, *10*, 9666–9677.
35. Johannsen, K.; Page, D.; Roy, S. A systematic investigation of current efficiency during brass deposition from a pyrophosphate electrolyte using RDE, RCE, and QCM. *Electrochim. Acta* **2000**, *45*, 3691–3702. [CrossRef]
36. De Almeida, M.; Barbano, E.; de Carvalho, M.; Tulio, P.; Carlos, I. Copper–zinc electrodeposition in alkaline-sorbitol medium: Electrochemical studies and structural, morphological and chemical composition characterization. *Appl. Surf. Sci.* **2015**, *333*, 13–22. [CrossRef]
37. Kumar, M.P.; Nidhi, M.; Srivastava, C. Electrochemical exfoliation of graphite to produce graphene using tetrasodium pyrophosphate. *RSC Adv.* **2015**, *5*, 24846–24852. [CrossRef]
38. Sylla, D.; Savall, C.; Gadouleau, M.; Rebere, C.; Creus, J.; Refait, P. Electrodeposition of Zn–Mn alloys on steel using an alkaline pyrophosphate-based electrolytic bath. *Surf. Coat. Technol.* **2005**, *200*, 2137–2145. [CrossRef]
39. Therese, G.H.A.; Kamath, P.V. Electrochemical synthesis of metal oxides and hydroxides. *Chem. Mater.* **2000**, *12*, 1195–1204. [CrossRef]
40. Konno, H.; Nagayama, M. Mechanism of electrodeposition of copper from cupric pyrophosphate solutions. *Electrochim. Acta* **1977**, *22*, 353–358. [CrossRef]
41. Kravtsov, V.; Kondratiev, V. Kinetics and mechanism of pyrophosphate metal complexes electroreduction. *Electrochim. Acta* **1991**, *36*, 427–434. [CrossRef]
42. Narkevicius, A.; Bucinskiene, D.; Samuleviciene, M.; Ramanauskas, R. Corrosion behaviour of Zn coatings electrodeposited from alkaline and acid solutions. *Trans. Inst. Met. Finish.* **2003**, *81*, 93–97.
43. Carlos, I.A.; de Almeida, M.R.H. Study of the influence of the polyalcohol sorbitol on the electrodeposition of copper–zinc films from a non-cyanide bath. *J. Electroanal. Chem.* **2004**, *562*, 153–159. [CrossRef]
44. El Meguid, E.A.; Awad, N.K. Electrochemical pitting corrosion behaviour of α-brass in LiBr containing solutions. *Corros. Sci.* **2009**, *51*, 1134–1139. [CrossRef]
45. Haciibrahimoglu, M.Y.; Yavuz, A.; Oztas, M.; Bedir, M. Electrochemical and structural study of zinc-rich brass deposited from pyrophosphate electroyte onto the carbon steel. *Dig. J. Nanomater. Biostruct.* **2016**, *11*, 251–262.
46. Ballesteros, J.; Torres-Martínez, L.; Juárez-Ramírez, I.; Trejo, G.; Meas, Y. Study of the electrochemical co-reduction of Cu^{2+} and Zn^{2+} ions from an alkaline non-cyanide solution containing glycine. *J. Electroanal. Chem.* **2014**, *727*, 104–112. [CrossRef]
47. Zeng, R.-C.; Zhang, J.; Huang, W.-J.; Dietzel, W.; Kainer, K.; Blawert, C.; Wei, K. Review of studies on corrosion of magnesium alloys. *Trans. Nonferr. Met. Soc. China* **2006**, *16*, s763–s771. [CrossRef]
48. Pardo, A.; Merino, M.C.; Coy, A.E.; Arrabal, R.; Viejo, F.; Matykina, E. Corrosion behaviour of magnesium/aluminium alloys in 3.5 wt. % NaCl. *Corros. Sci.* **2008**, *50*, 823–834. [CrossRef]
49. Stern, M.; Geary, A.L. Electrochemical polarization I. A theoretical analysis of the shape of polarization curves. *J. Electrochem. Soc.* **1957**, *104*, 56–63. [CrossRef]
50. Liang, J.; Srinivasan, P.B.; Blawert, C.; Dietzel, W. Comparison of electrochemical corrosion behaviour of MgO and ZrO_2 coatings on AM50 magnesium alloy formed by plasma electrolytic oxidation. *Corros. Sci.* **2009**, *51*, 2483–2492. [CrossRef]
51. Sorensen, C.D.; Nelson, T.W. Friction stir welding of ferrous and nickel alloys. *Frict. Stir Weld. Process.* **2007**. [CrossRef]
52. Lee, W.-B.; Jung, S.-B. The joint properties of copper by friction stir welding. *Mater. Lett.* **2004**, *58*, 1041–1046. [CrossRef]
53. Feliu, S.; Samaniego, A.; Barranco, V.; El-Hadad, A.A.; Llorente, I.; Adeva, P. The effect of low temperature heat treatment on surface chemistry and corrosion resistance of commercial magnesium alloys AZ31 and AZ61 in 0.6 M NaCl solution. *Corros. Sci.* **2014**, *80*, 461–472. [CrossRef]